Understanding basement fracture architecture in Padra Field, South Cambay Basin, India, through full-azimuth imaging

Abhinandan Ghosh[1]

https://doi.org/10.1190/tle38040262.1.

Abstract

Detection and characterization of fractures in reservoirs is of great importance for maximizing hydrocarbon productivity and recovery efficiency. Fractures play an important role in the producibility of unconventional reservoirs such as basement reservoirs. Basement reservoirs are typically found within metamorphic and igneous rock underlying a sedimentary basin, where faulting and tectonic uplift has led to creation of a fracture network. For fracture characterization, integration of information from seismic and nonseismic data such as cores and/or formation microimaging (FMI) logs is essential. Various seismic attributes such as coherency and curvature that are derived from reflection seismic data have been used for more than a decade to detect faults and fractures. In advanced seismic fracture detection technology, automatic fault extraction (AFE) from diffraction seismic data (discontinuity volume) more effectively detects finer scale features in seismic data. We demonstrate the utility of this methodology with an application to seismic data from the Padra Field, South Cambay Basin, India, where the basaltic Deccan Trap forms the basement, and hydrocarbons are produced from basement fractures. Diffraction imaging was applied during processing of the full-azimuth 3D-3C seismic data that cover this field. Using wavefield decomposition in the subsurface local angle domain, separate reflection (specular) and diffraction data volumes were produced. The high-resolution specular stack data imaged a prominent reflector well below the trap top, which is not visible in conventional seismic reflection data. Diffraction stack data also provided higher resolution fault definition and enhanced imaging of spatially consistent geological discontinuities. Subsequent application of the AFE technique to diffraction-imaged data yielded sharp and crisp definition of faults and fractures. We also performed velocity variation with azimuth analysis of 3D angle-azimuth reflection gathers to generate a fracture orientation map. Both sets of results were validated by fractures detected in FMI logs from wells in the field.

Introduction

In geology, basement is defined as any rock below a sedimentary section that is metamorphic or igneous in origin. Basement rocks, typically basalts or granite, are hard and brittle, having little to no matrix porosity and permeability. When basement structures are deformed through tectonic action, seismic-scale faults and subseismic-scale fractures and fracture networks are created. Under the right conditions, significant volumes of hydrocarbons can accumulate in the void space created by these basement fractures. Fractured and weathered basement reservoirs are a known play type worldwide. Several basins in India have fields that produce from fractured basement reservoirs — Assam and Assam Arakan Basin, Mumbai Basin, Krishna Godaveri Basin, Cauvery Basin, and Cambay Basin.

Depending on the depth of burial, seismic reflections from the basement can be weak and masked by several types of noise including multiples. Enhancing the seismic response at the basement level is therefore important to assess basement prospectivity. Conventional imaging procedures tend to be biased toward higher energy events such as reflections from stratal boundaries or discontinuities such as faults. This energy is referred to as "specular" energy, and it typically dominates the seismic data volume. But a significant amount of energy associated with finer scale features such as small faults, fractures, stratigraphic edges, reservoir heterogeneities, etc., are also recorded in the form of "diffraction" energy. Information contained in diffraction energy arising from such features can be particularly valuable for reservoir characterization, for example, in identifying subtle changes that cause reservoir compartmentalization or for mapping the fracture network in fractured basement reservoirs. Unfortunately, such fine-scale seismic events tend to be masked by the dominant specular energy events in seismic data, and they are also irretrievably lost during conventional seismic processing.

"Diffraction imaging" is an alternative processing procedure that aims to attenuate the reflection energy, leaving behind any focused diffraction events generated by faults, unconformities, and depositional discontinuities. The ability to decompose the specular and diffraction energy from the total scattered field contained within a full-azimuth directional gather is the core component of the diffraction imaging system. The process uses point diffractor ray tracing, which ensures maximum illumination of image points from all subsurface directions and all surface source-receiver locations, accommodating all arrivals (Koren and Ravve, 2011). Data are depth migrated in the local angle domain (LAD), where the entire wavefield of recorded seismic data is used to generate "true-amplitude" angle-dependent, or angle-and-azimuth-dependent image gathers in the subsurface angle domain rather than the surface offset domain. Managing multipathing in wave propagation produces better images in complex geology than the usual Kirchhoff migration, which assumes a single arrival.

This paper describes our workflow for characterizing the fractured basement reservoir of the Padra Field in the South Cambay Basin in western India (Figure 1). We processed the full-azimuth 3D seismic data over a part of the field (the Phase-I area, covering 50 km^2) to obtain both specular and diffraction images, and we used the resultant data to compute seismic attributes that visualize fractures and fracture networks in the basement. These were then validated against fractures interpreted in formation microimaging (FMI) data in wells.

[1]SPIC, Oil and Natural Gas Corporation Ltd., Mumbai, India. E-mail: ghosh_a1@ongc.co.in.

Background geology

Cambay Basin is a narrow, elongated intracratonic rift graben situated in the northwestern part of the Indian Peninsula, straddling the states of Gujarat and Rajasthan and extending from the Luni River in the north to the Tapi River in the south. Cambay Basin is believed to have formed during Early Cretaceous time due to rifting along Dharwarian orogenic trends during the northward migration of the Indian plate after its breakup from Gondwanaland in Late Triassic–Early Jurassic time (Biswas, 1982). The major longitudinal faults are aligned with the Dharwarian trend, running parallel to the basin trend. The basin contains five intrabasinal uplifted blocks created by a transverse fault system.

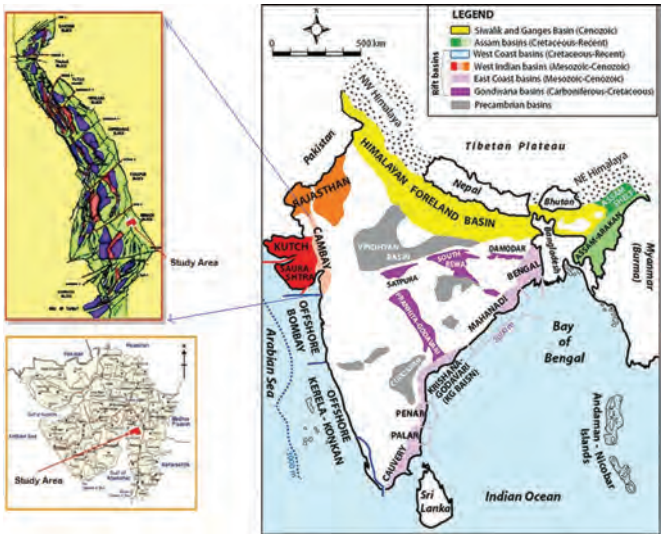

Figure 1. Location map of survey area displayed on tectonic map of Cambay Basin (top left) and on political map of the northwestern part of India (bottom left). Location map of Cambay Basin on the map of India (right).

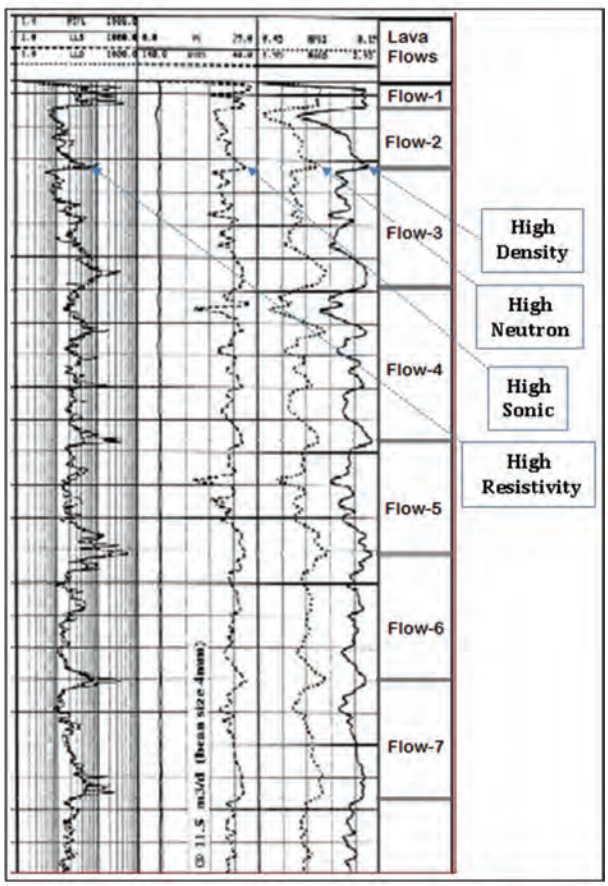

Figure 2. Well logs within the Deccan Trap (basement) section in Padra Field: resistivity-photo electric-sonic-neutron-density. Note the cyclic pattern in the neutron-density log associated with episodic lava flows.

The Padra structure lies in the northeastern rising flank of the late Tertiary Broach Depression in the South Cambay Basin (Figure 1). The structure shows a series of subparallel north-northwest–south-southeast-trending normal faults forming successive horsts and grabens and having many fault-bound structures within it. In general, wells lying on the horsts have encountered oil in basement penetrations, while those falling in grabens are dry in the basement. Stratigraphically, the basin contains a 600–700 m thick Tertiary- to Quaternary-age sedimentary section unconformably overlying the Deccan Trap (volcanics) basement. The Tertiary-age section in the study area contains the Dadhar, Ankleshwar, and Olpad formations. The fractured and weathered traps are the unconventional reservoirs in this field. They contain oil columns up to 300 m thick. Tight trap layers, and the overlying shales of the Olpad Formation, act as the seal.

The Deccan Trap basement is composed of layered basalts laid down by episodic lava flows that occurred during the Paleocene to Upper Cretaceous period. These different lava flows are recognizable in the Deccan Trap section by their characteristic cyclical nature in density-neutron well logs (Figure 2) (Kumar, 2009). Resistivity and sonic logs also show similar alternating high-resistivity/velocity, low-resistivity/velocity layering (Jamkhindikar et al., 2013). The bottom of each flow layer is massive basalt, grading into weathered basalt toward the top.

Data

Padra Field is covered by 3D seismic data acquired in three phases during 2009–2010, 2014–2015, and 2015–2016. Field data from these three vintages were merged and processed through prestack time migration in 2016. Common-midpoint (CMP) gathers from the merged data set have 360° source-receiver azimuthal distribution, ideal for full-azimuth subsurface angle decomposition; these were used as input data for the present study.

Oil was discovered in Padra Field both in Ankleshwar and trap formations many decades ago, in 1961. So far, 124 wells have been drilled in the field, of which 67 are exploratory wells and 57 are development wells. Of these, 99 wells are hydrocarbon bearing, and 25 wells are dry and abandoned. Conventional logs, including dipole sonic imager from 105 wells (of which 27 are deviated) were used in the present study. FMI logs are available in 10 wells in the Phase-I area. Basement hydrocarbon reserves at Padra Field are estimated to be 0.68 million metric tons of which 0.42 million metric tons have already been produced.

Method

It is known that different fault blocks within the Cambay Basin have different oil habitats. Thus, understanding the orientation of these faults and associated fracture patterns is essential to efficiently exploit the hydrocarbons contained in tight reservoirs

of the basin. Padra Field is currently under production, but there are areas of exploratory interest that remain within its mapped most likely area. The observed nature of occurrence of oil and gas within the unconventional basement reservoirs of Padra Field demonstrates that hydrocarbon entrapment is not governed by structural closure, which causes significant uncertainty in identifying leads and prospects to drill. It is well established that porosity, permeability, and hydrodynamic behavior of the basement reservoir at Padra Field are related to the natural fractures present in it. The basement basalt flows do not result in massive crystalline layers with zero porosity, but rather form alternations of crystalline and porous layers due to formation of vesicles. Another important phenomenon providing permeability is fracture development due to differential cooling rates of the upper and lower surfaces of a lava flow layer compared to its interior. The vesicular layers become weak planes along which the natural fractures propagate, providing connectivity between vesicles. Hydrocarbon can migrate through these fractures and accumulate within the vesicles.

The existing reservoir model for Padra Field does not adequately explain the observed presence or absence of hydrocarbons in well penetrations of the basement or the differences in rates of producing wells. This is most likely due to inaccurate characterization of the fracture network in the basement reservoir. There is still ample scope for exploratory activities in the Padra area. In this paper, we describe a workflow designed to better image the basement and fine-scale features within the basement at Padra Field. The main steps of this workflow are:

1) building an effective velocity model using sonic logs from 50 wells down to trap top and performing velocity scans and tomography within the trap to image the section below the trap top
2) full-azimuth subsurface angle domain directional gather decomposition of full-azimuth 3D land seismic survey data
3) specular amplitude enhancement in the subsurface LAD to image the intratrap section
4) enhanced diffraction imaging by applying an appropriate diffraction filter to directional gathers
5) applying the automatic fault extraction (AFE) procedure to enhance diffraction image data
6) validation of seismically imaged fractures with FMI log data at well locations where these logs are available
7) determination of fracture orientation based on velocity variation with azimuth (VVAZ) analysis of 3D reflection angle-azimuth gathers and subsequent validation with FMI log data where available.

Data conditioning

As a first step, residual static correction was done in the shot domain to optimize the alignment of shallow reflections. Next, noise attenuation was done successively in shot, receiver, and CMP domains.

Velocity model building

Sonic logs show a large increase of velocity when going from the overlying sediments of the Olpad Formation into basement (Figure 3). Using 50 suitably filtered sonic logs from the area, a geostatistical velocity model was built from floating datum to 500 m below the trap top, as shown in Figure 4a. Though sonic logs do not have any deeper information below trap top, every sonic log shows a very high trend of sonic interval velocity from Olpad/trap top formation, as shown in Figure 3. This high interval velocity is quite natural in a basaltic environment. Velocity flooding was done within the basement section using the high interval velocities obtained from sonic logs, with the aim of imaging intratrap reflections. Next, the velocity models of the two zones (shallow sedimentary and deeper basement) were merged. Finally, velocities were updated using tomography to obtain the final velocity model (Figure 4b).

LAD prestack depth migration

Seismic data recorded at the acquisition surface were decomposed (mapped) into four-dimensional in-situ subsurface LAD space: dip ($v1$), and azimuth ($v2$) of the ray-pair normal, opening angle ($\Upsilon 1$), and opening azimuth ($\Upsilon 2$). For each direction of the resultant 5D directional gather, seismic data events corresponding to ray pairs with the same orientation of the reflecting surface, but having different opening angles, are accounted for in weighted summation form. The directional gathers contain directivity-dependent information about both specular and diffraction energy at each subsurface point. For example, a reflection gather at well A (Figure 5) has been azimuthally sorted so that traces fall in six azimuthal sectors of 30° each. These azimuthal gathers show the characteristic wavy reflection pattern indicative of azimuthal anisotropy. These gathers are now suitable for VVAZ analysis.

Specular amplitude enhancement in LAD

Full-azimuth direction gathers contain directivity-dependent information at each subsurface point, which allows for

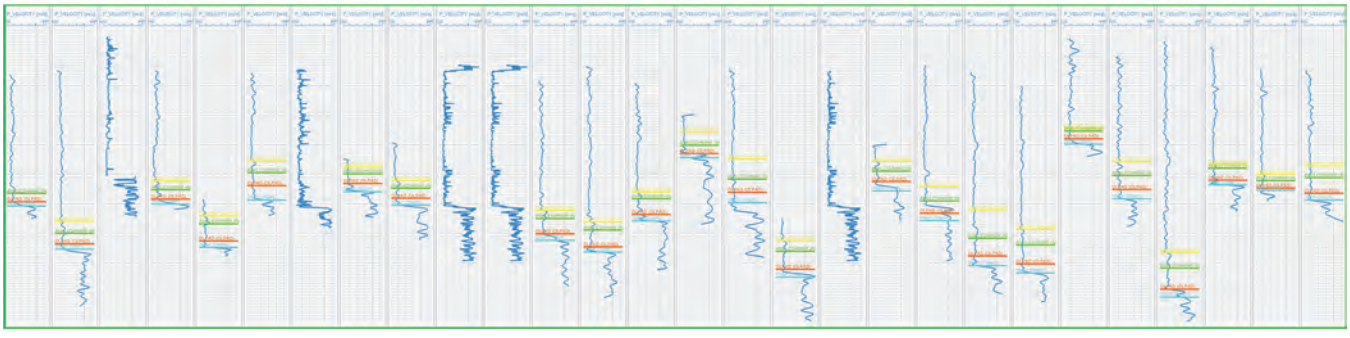

Figure 3. Sonic logs with four markers (Dadhar-Ankleshwar-Olpad-Trap) from multiple wells showing the typical increase in velocity going from overlying sedimentary section into the trap (basement) section.

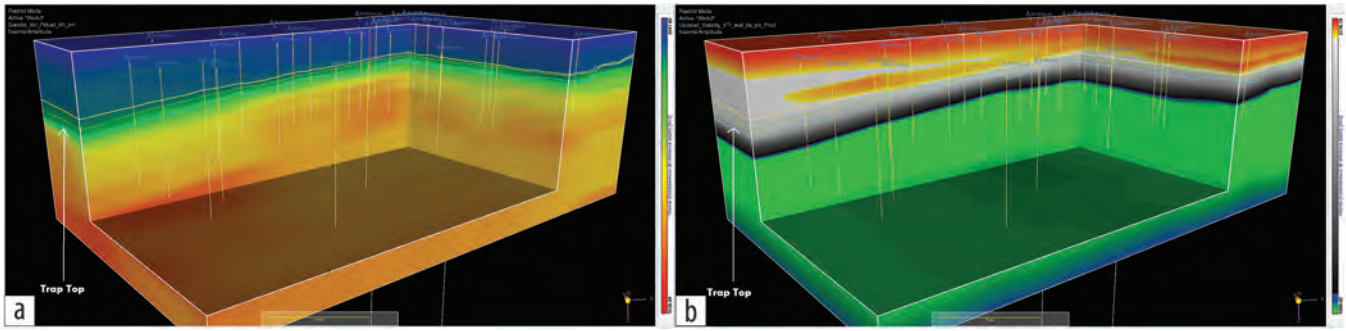

Figure 4. (a) Initial velocity model generated using 50 sonic logs. (b) Final velocity model generated by merging sedimentary and basement velocity sections.

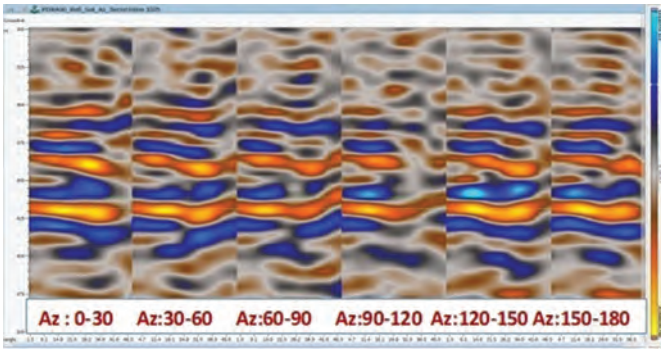

Figure 5. Azimuthal sectoring of reflection gather at well A location.

enhancement of subsurface feature images by applying a different specular/diffraction weighted filter to create a specular (continuous structural surface)/diffraction (discontinuous objects like fractures, and small-scale faults) stack (Koren and Ravve, 2011; Ravve and Koren, 2011). Figure 6 shows an example of a full-azimuth 3D directional gather that represents the specular directions at different depth points. Specular reflections well below trap top are distinctly visible in specular stack data. To generate this, we applied weighted filters on LAD generated directional gathers in two different ways:

1) **Specular filtering.** Enhancement of specular energy only, discarding all kinds of diffraction energy and noise, generating a specular stack. The high energy values associated with the specular directions can be used to obtain more detailed and sharpened images. Figure 7 compares a vintage conventionally imaged reflection stack section with the equivalent specular stack section. Note the prominent sub-trap top reflection that is visible in the specular stack data. The sub-trap top reflector confirms that Deccan Trap basement is composed of layered basalts laid down by episodic lava flows. The new data has enabled visualization and interpretation of basement architecture at Padra Field.
2) **Diffraction filtering.** To achieve this, specular energy is first muted at a specified angular aperture, after which the remaining diffraction energy is enhanced, generating a diffracted stack. The diffraction volume shows enhanced imaging of spatially consistent geological discontinuities and higher resolution fault definition. The diffraction depth slice in Figure 8a shows sharp definition of intratrap fault patterns. Distinct differences in fault pattern across the intersection of the depth slice with the trap top (shown by green line) are clearly observed.

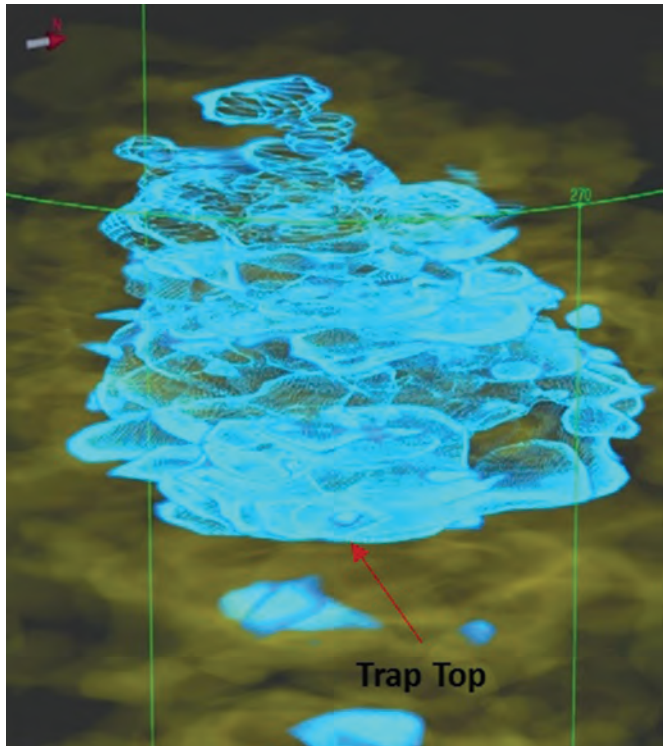

Figure 6. 3D view of full-azimuth directional gather showing specular directions at different subsurface depth points. Note the imaging of intratrap events.

Automatic fault extraction

The AFE technique was applied to the diffraction volume to extract and enhance linear and planar fault-related features. Figure 8b shows the same depth slice as in Figure 8a, after application of AFE. Here, faults have been separated from other discontinuity features in the diffraction stack data, and they are now sharply defined. Figure 9 compares the ant-track attribute extracted for the 725 m depth slice from conventional reflection seismic data (Figure 9a), with the same derived from diffraction stack data (Figure 9b). Clearly, fault and fracture patterns can be derived in a more reliable and geologically meaningful way using the diffraction (discontinuity) data than the conventional reflection (continuity) data.

Validation of results

Seismic fault/fracture plane extraction compared with data from FMI logs. Fault/fracture plane interpretations made from AFE analysis match well with fracture data from FMI logs. Here we compared: (1) AFE azimuth vector at well locations only;

(2) fault/fracture orientation rose diagram derived from various diffraction depth slices (approximately 1 km^2) surrounding the well; and (3) FMI fracture rose diagram at well location only.

For well #PDRA-XX, in Figures 10a–10c

- AFE azimuth vector at the well location is oriented at 149° at depth of 610 m.
- Diffraction seismic shows azimuth range of 147°–158° for a depth range 610–615 m.
- FMI log shows azimuth range of 146°–152° for depth range 612–613 m.

For well #PDRA-YY, in Figures 10d–10f

- AFE azimuth vector at the well location is oriented at 132° at depth of 665 m.
- Diffraction seismic shows azimuth range of 131.5°–157.5° at depth of 665 m.
- FMI log shows azimuth range of 131°–152° for depth range 665–666 m.

Fault/fracture plane orientation derived from VVAZ analysis of imaged reflection gathers compared with data from FMI logs. Considering the fractured trap top reflection interval to be an orthorhombic anisotropic layer within a vertically transverse isotropy background, VVAZ analysis was done on 3D angle-azimuth reflection gathers, and three anisotropy related attribute volumes (Koren and Ravve, 2014) were created:

1) Alpha slow: residual moveout along the fracture symmetry axis
2) Delta alpha: difference between residual moveout along fracture symmetry axis and fracture orientation axis (fracture intensity)
3) Azimuth slow: azimuth of fracture symmetry axis (fracture orientation)

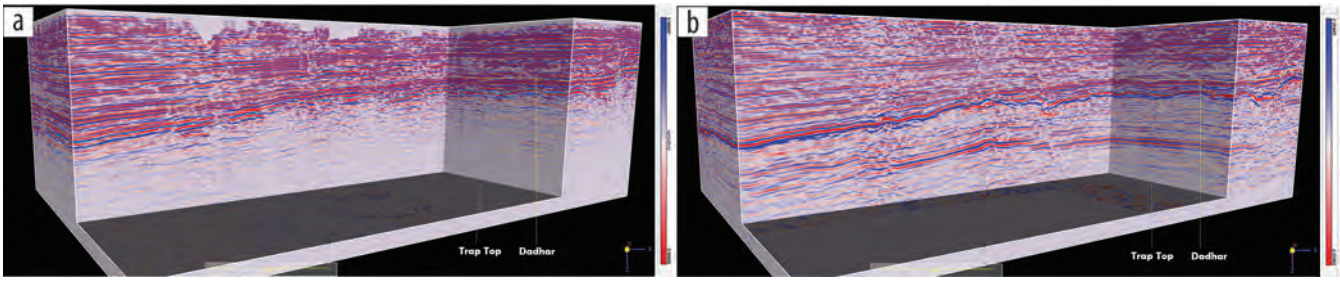

Figure 7. (a) Vintage reflection stack. (b) Specular stack showing well-imaged sub-trap top reflection.

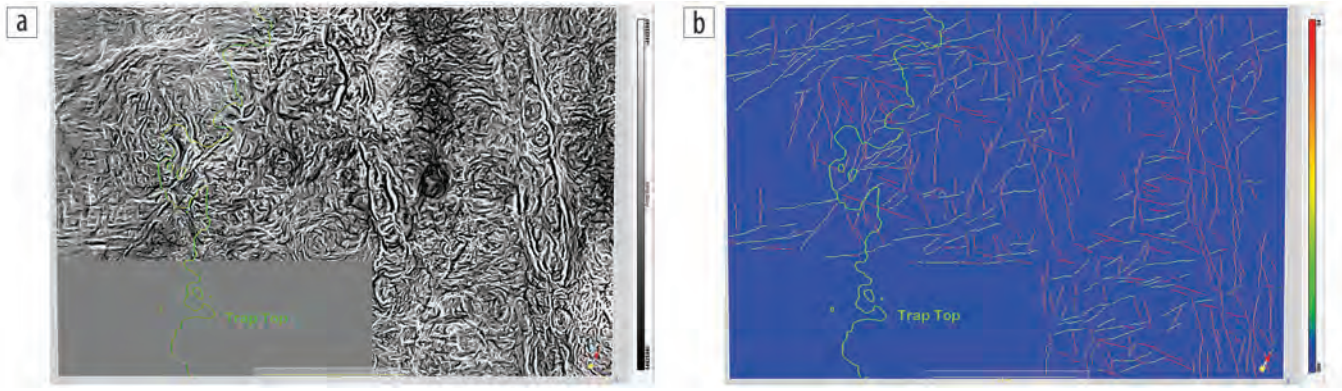

Figure 8. (a) Depth slice at 725 m from diffraction stack showing trap top intersection (green line). (b) Same depth slice after application of AFE showing enhanced definition of faults.

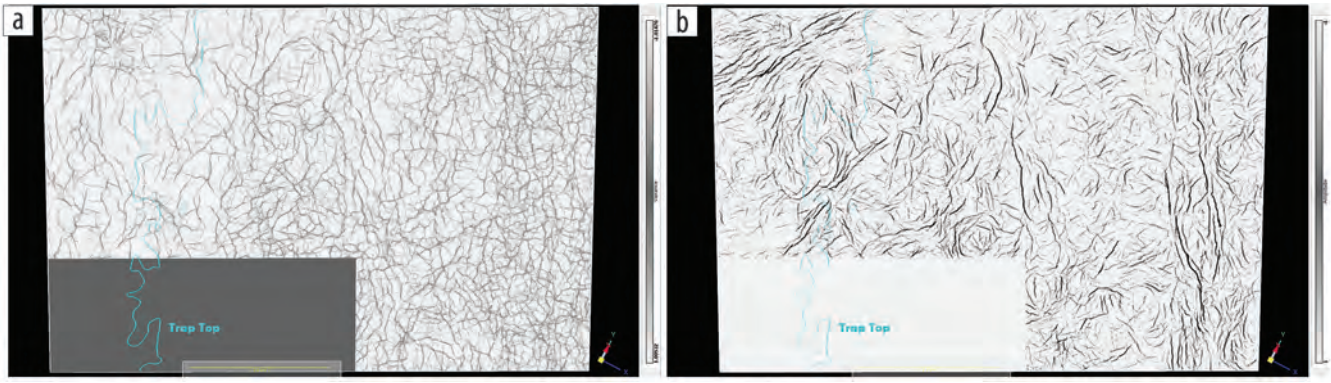

Figure 9. (a) Ant track from vintage reflection seismic data depth slice at 725 m with trap top shown in blue. (b) The equivalent from diffraction seismic data.

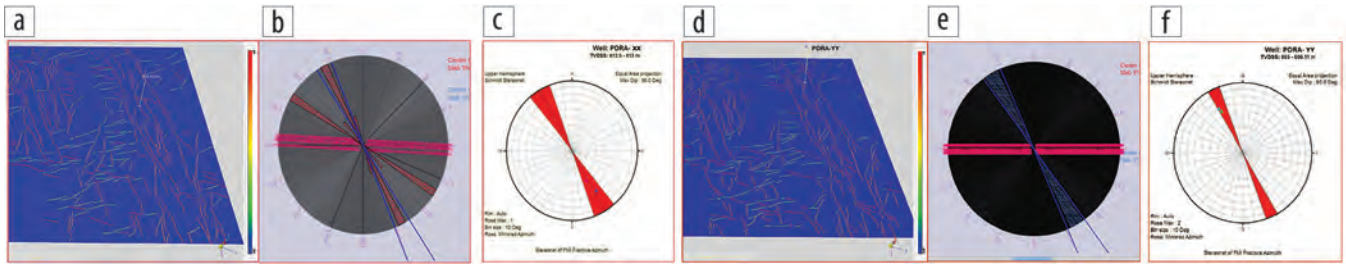

Figure 10. Fracture orientation data from (a–c) well #PDRA-XX and (d–f) well #PDRA-YY. (a, d) AFE vector azimuth, (b, e) diffraction rose diagram, and (c, f) FMI rose diagram.

We used the aforementioned data to generate fracture intensity and orientation maps and associated rose diagrams below the trap top level. These fracture orientations match very well with the fracture orientation stereonet calculated for well #PDRA-ZZ, located in the southeastern part of the study area (Figure 11).

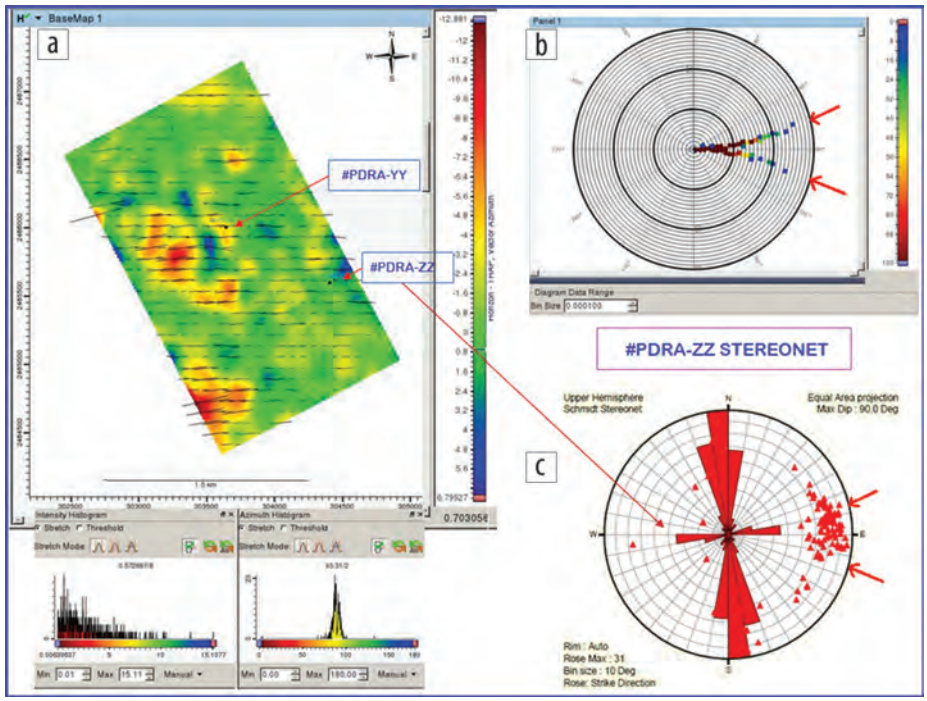

Figure 11. (a) Fracture orientation map with (b) associated rose diagram extracted from VVAZ analysis of diffraction seismic data at 530 m depth and (c) FMI rose diagram at depth range 522–563 m from well #PDRA-ZZ.

Conclusions

The Padra Field in South Cambay Basin produces hydrocarbons from fractured basement. To optimize field development, it is necessary to accurately characterize these fractures. With this as an objective, the full-azimuth seismic survey data covering Padra Field was processed and imaged with wavefield decomposition in the LAD. Products included an enhanced specular reflection amplitude volume with good imaging of the intratrap section and a high-resolution diffraction volume for detection of small faults and fractures. The diffraction (discontinuity) volume yields seismic attributes that have performed better compared to the coherency and curvature attributes from conventionally processed seismic data in the Padra area, for fracture detection. Additionally, VVAZ analysis of angle-azimuth reflection gathers from the LAD imaged data enabled mapping of basement fracture orientation and intensity. AFE analysis of the diffraction volume yielded a basement fracture network that has been validated with fracture data derived from FMI logs in the field.

The fracture density map produced from executing our workflow is being used for continued development of the fractured basement reservoir at Padra Field in optimizing both new well placement and for design of well trajectories. TLE

Acknowledgments

The author sincerely thanks Shri A. K. Dwivedi, Director (Exploration), ONGC, India for permission to publish this paper. The views expressed here are exclusively those of the author only, and they need not necessarily match with official views of ONGC.

Data and materials availability

Data associated with this research are confidential and cannot be released.

Corresponding author: ghosh_a1@ongc.co.in

References

Biswas, S. K., 1982, Rift basins in western margin of India and their hydrocarbon prospects with special reference to Kutch Basin: AAPG Bulletin, **66**, no. 10, 1497–1513.

Jamkhindikar, A., M. Jain, and S. N. Mohanty, 2013, Hydrocarbon prospectivity of Deccan Trap in northern Cambay Basin: 10th Biennial International Conference and Exhibition, SPG, https://www.spgindia.org/10_biennial_form/P167.pdf, accessed 18 March 2019.

Koren, Z., and I. Ravve, 2011, Full-azimuth subsurface angle domain wavefield decomposition and imaging Part I: Directional and reflection image gathers: Geophysics, **76**, no. 1, S1–S13, https://doi.org/10.1190/1.3511352.

Koren, Z., and I. Ravve, 2014, Azimuthally dependent anisotropy velocity model update: Geophysics, **79**, no. 2, C27–C53, https://doi.org/10.1190/geo2013-0178.1.

Kumar, A., 2009, Reservoir nature and evaluation of Deccan Trap basement, Cambay Basin, India: Presented at the 2nd SPWLA-India Symposium.

Ravve, I., and Z. Koren, 2011, Full-azimuth subsurface angle domain wavefield decomposition and imaging: Part 2 — Local angle domain: Geophysics, **76**, no. 2, S51–S64, https://doi.org/10.1190/1.3549742.